



Physics in High Magnetic Fields / Physique en champ magnétique intense

Resonance THz spectroscopy in high magnetic fields

*Spectroscopie de résonance THz en champ magnétique intense*Anne-Laure Barra^a, Michel Goiran^b, Roberta Sessoli^c, Sergei A. Zvyagin^{d,*}^a Laboratoire national des champs magnétiques intenses-Grenoble, CNRS-UJF, BP 166, 38042 Grenoble, France^b Laboratoire national des champs magnétiques intenses-Toulouse, INSA UPS UJF CNRS, UPR 3228, université de Toulouse, 31400 Toulouse, France^c Dipartimento di Chimica, Università degli Studi di Firenze, 50019 Sesto Fiorentino, Italy^d Dresden High Magnetic Field Laboratory (HLD), Helmholtz-Zentrum Dresden-Rossendorf, 01314 Dresden, Germany

ARTICLE INFO

Article history:

Available online 11 January 2013

Keywords:

ESR
EPR
Spectroscopy
High magnetic field

Mots-clés :

ESR
RPE
Spectroscopie
Champ magnétique intense

ABSTRACT

The employment of the high-magnetic-field resonance spectroscopy to probe magnetic excitations in the THz frequency range is reported. To illustrate the great potential of this technique in solid state physics, we present results of recent electron spin resonance studies of the quantum-tunneling effect in the single-molecule magnet Mn12tba and of the soliton-magnon crossover in Cu-PM, a spin-1/2 Heisenberg chain system with a staggered transverse field. Among others, we report on the successful use of the THz-range time-domain and free electron laser spectroscopy to study magnetic excitation spectra in pulsed magnetic fields.

© 2012 Académie des sciences. Published by Elsevier Masson SAS. All rights reserved.

R É S U M É

Cet article décrit l'utilisation de spectroscopie de résonance en champ magnétique intense pour sonder les excitations magnétiques dans la gamme des fréquences THz. Afin d'illustrer le grand potentiel de cette technique en physique de l'état solide, nous présentons des résultats récents obtenus par résonance de spin électronique lors d'études sur l'effet tunnel quantique dans la molécule-aimant Mn12tba ainsi que l'étude de la transition soliton-magnon dans Cu-PM, une chaîne de spin-1/2 de Heisenberg possédant un champ transverse alterné. Ensuite, l'apport de la spectroscopie THz dans le domaine temporel et de la spectroscopie à base de rayonnement laser à électrons libres pour l'étude des spectres d'excitations magnétiques en champ magnétique pulsé est présenté.

© 2012 Académie des sciences. Published by Elsevier Masson SAS. All rights reserved.

1. Introduction

The electromagnetic-wave spectrum between 300 GHz and 3 THz (ca. 1.2–12 meV; 10–100 cm⁻¹; 14–140 K), known as “THz gap”, represents a very important domain for condensed matter physics and material science spectroscopy, in particular for the resonance spectroscopy in magnetic fields. Depending on the nature of magnetic excitations, one can distinguish between electron spin resonance (ESR) and cyclotron resonance (CR) phenomena. ESR [sometimes called electron

* Corresponding author.

E-mail addresses: anne-laure.barra@lncmi.cnrs.fr (A.-L. Barra), michel.goiran@lncmi.cnrs.fr (M. Goiran), roberta.sessoli@unifi.it (R. Sessoli), s.zvyagin@hzdr.de (S.A. Zvyagin).

paramagnetic resonance (EPR)] is based on the detection of resonance absorption of electromagnetic radiation corresponding to transitions between electron-spin energy levels split by internal effects (crystal-field anisotropy, exchange interactions, etc.) and/or by an applied magnetic field (known as the Zeeman effect). It is worth to mention that the use of commercially available fixed-frequency ESR spectrometers is not well suited when studying magnetic materials with a large zero-field-splitting, complex frequency-field diagrams of magnetic excitations, or field-induced phase transitions. That is why the employment of ESR spectrometers capable to operate in high magnetic fields and at multiple frequencies is of particular importance when examining magnetic excitation spectra in such systems. Compared to ESR, CR corresponds to transitions between Landau levels, split by magnetic field. Despite of different natures of ESR and CR, the techniques used to study these phenomena can be essentially the same.

The remainder of this article is organized as follows. To illustrate the great potential of high-field THz-range ESR spectroscopy we report the application of this technique to two classes of magnetic materials, namely single-molecule magnets (Section 2) and spin chains (Section 3). The low-temperature magnetic behavior of these magnetic systems is dominated by quantum effects, which are rather different in their origins. In Section 4 the review of novel experimental approaches (including pulsed-field THz-range time-domain spectroscopy and ESR spectroscopy with a free electron laser employed as a source of THz radiation) to study resonance phenomena in solids is given.

2. Quantum tunneling of the magnetization in single-molecule magnets

As an example illustrating the application of high-field ESR spectroscopy in condensed matter physics, we focus on a special class of molecules, where the intramolecular exchange interaction between the paramagnetic centers of the molecules stabilizes a large-spin ground state [1]. This, combined with uniaxial magnetic anisotropy, gives rise to an energy barrier that hampers the reversal of the magnetization at low temperature. The resulting magnetic bistability (magnetic hysteresis) is at the origin of the evocative term Single-Molecule Magnets (SMM) under which these systems are generally known. Here we illustrate the use of high-field ESR for the analysis of static magnetic properties [2] but high-field ESR also allows studying decoherence effects in SMM [3,4].

The simplest Hamiltonian to describe the uniaxial magnetic anisotropy is

$$\mathcal{H} = \mu_B \mathbf{B} \mathbf{g} \mathbf{S} + D S_z^2 \quad (1)$$

where S is the spin ground state of the molecule and D is also known as the axial zero-field-splitting (ZFS) parameter. The effect of a negative D , $D = -0.4 \text{ cm}^{-1}$, on the $S = 10$ multiplet of a strictly tetragonal cluster of the archetypal Mn12 cluster family (abbreviated as Mn12tba with acetate ligand replaced by *t*-butyl-acetate) is shown in Fig. 1 [5,6]. The same figure shows the effect of an axial field on the energy-level spectrum, while the red (vertical) lines represent the resonance fields for $\Delta m_S = \pm 1$ transitions, observed in the ESR spectrum recorded at 360 GHz. The $2S$ resonance lines calculated with Eq. (1) are regularly spaced and the field separation is $\Delta H = D/(g\mu_B)$ [2]. It is clearly evident how informative an ESR spectrum of an SMM can be, provided that large fields and tunable frequencies are available. Indeed, the entire spectrum of a polycrystalline powder of the archetypal Mn12ac SMM (where *ac* = acetate) extended over $\sim 18 \text{ T}$ and required the use of a hybrid magnet combining a resistive magnet based on Bitter and polyhelix coils with a superconductor solenoid so that a maximum field of 30 T was available [7].

In the case of Mn12tba, the single crystal ESR spectrum recorded in axial fields is shown in the upper part of Fig. 2, with an exciting frequency of 345 GHz generated by a 115 GHz Gunn oscillator equipped with a tripler. The ESR signal is then recorded with the help of an InSb bolometer. The major difference between the experimental spectrum and the scheme of Fig. 1 is that the resonances are not equally spaced [8]. This is a direct consequence of the rough approximation done when using Eq. (1). The magnetic anisotropy, when expressed as a multipolar expansion, would in principle require terms up to the $(2S)$ -th order, which are classified according to the symmetry of the system by using the Stevens operators [9]. In the case of a tetragonal system and limiting the series to the sixth order, the spin Hamiltonian becomes:

$$\mathcal{H} = \mu_B \mathbf{B} \mathbf{g} \mathbf{S} + D S_z^2 + B_4^0 \mathbf{O}_4^0 + B_6^0 \mathbf{O}_6^0 + B_4^4 \mathbf{O}_4^4 + B_6^4 \mathbf{O}_6^4 \quad (2)$$

where \mathbf{O}_n^m are the Stevens operators and D , B_n^m are the crystal-field parameters defining the anisotropy of the system. While n refers to the total order of the operator, m indicates the order in $S_+ S_-$ terms.

The terms \mathbf{O}_n^m with $m = 0$ only modify the level splitting and change the separation between resonances compared to Fig. 1 as indeed observed for Mn12tba. More important is the effect of terms with $m \neq 0$. They are related to the transverse anisotropy and are responsible for the admixing of levels on opposite sides of the anisotropy barrier and, therefore, of the efficiency of the tunnel mechanism. It is important to stress here that, although terms of growing order are associated with smaller and smaller parameters, their efficiency in promoting tunneling between the pair of ground states is relevant. In fact, the tunnel rate is influenced by the different B_n^m terms at the $(2S/m)$ -th order of perturbation. Very small terms with large m thus dominate the quantum behavior.

The quantification of these very small parameters is a challenging task for which ESR has demonstrated to be particularly useful, comparable only with inelastic neutron scattering [10,11]. Even more important is, however, to understand the origin of higher order terms of the magnetic anisotropy. Single crystal ESR spectra recorded in the *ab* plane of the tetragonal crystal of Mn12tba have provided very precious hints. In Fig. 2, we report the angular dependence of the spectra recorded

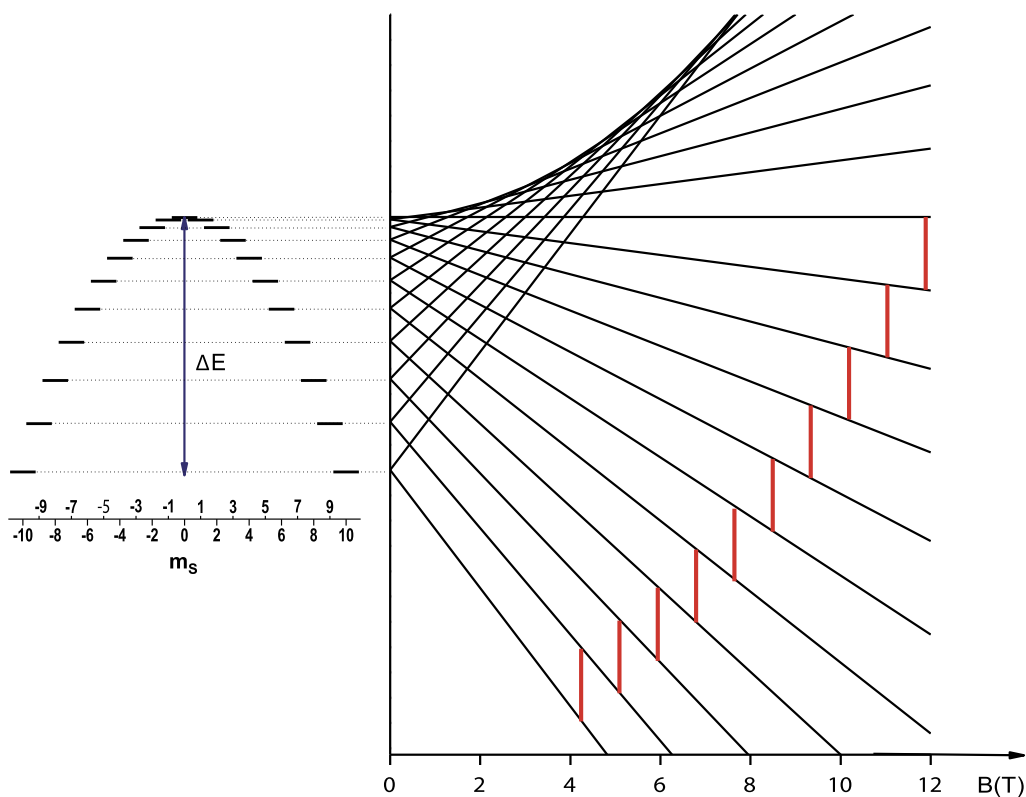


Fig. 1. (Color online) Left part: energy diagram in zero magnetic field of the spin ground state $S = 10$ split by a negative axial ZFS, D ; right part: the Zeeman effect on these levels for a magnetic field applied along the molecular symmetry axis. The red lines show the transitions expected at 360 GHz.

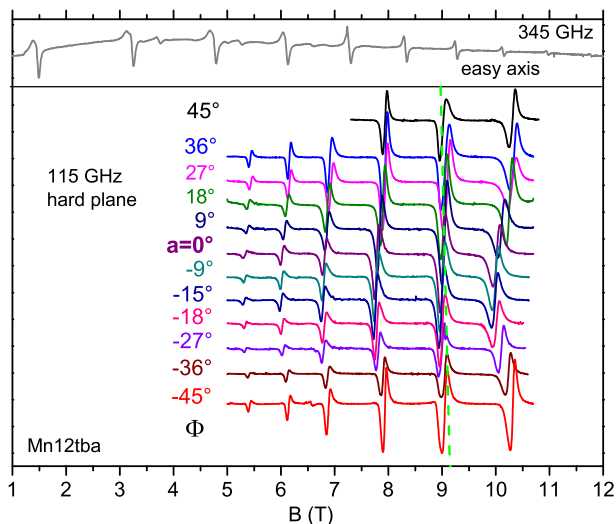


Fig. 2. (Color online) Top: the ESR spectrum recorded at 30 K and 345 GHz on a single crystal of $Mn_{12}tba$ with the field along the crystallographic c axis. Bottom: ESR spectra recorded at 5 K and 115 GHz when the field is applied in the ab plane at a variable angle Φ from the a axis. The green dotted line underlines the absence of an orientation dependence of the transition at the second-highest field.

by spanning the hard plane. A 90° periodicity of the resonance of each line is observed, in agreement with the tetragonal symmetry. Noteworthy is the fact that the angular dependence is not homogeneous over the resonance involving different levels of the $S = 10$ manifold. The transition at the second-highest field, the one formally involving $m_S = -9$ and $m_S = -8$ states, is practically isotropic in the ab plane. This behavior can be reproduced by introducing a non-zero B_6^4 parameter.

This sixth-order term cannot be brought in by the single spins constituting the cluster, as the largest individual spin, $s = 2$ for $Mn(III)$, would allow only fourth-order contributions. In order to verify if the multi-spin nature of the cluster plays

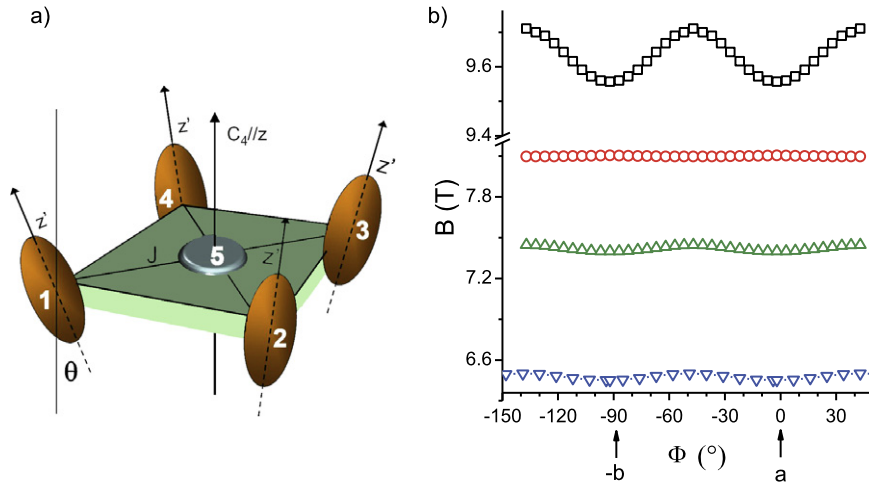


Fig. 3. (Color online) (a) Schematic view of the multi-spin model employed to simulate the ESR spectra of Mn12tba. Five $s = 2$ spins, labeled in white, are ferromagnetically coupled with the coupling constant J . The easy axis of the symmetry-related spin centers 1–4 forms an angle θ with the C_4 symmetry axis, while the central one is fully axial. (b) Calculated angular dependence in the ab plane of the four highest-field ESR resonances.

a role, the resonance lines have been calculated assuming a more complex spin Hamiltonian, where magnetic exchange and anisotropy are treated at the same level [8]. In order to reduce the Hilbert space dimension from the 10^8 required to handle the eight $s = 2$ and the four $s = 3/2$ spins constituting the Mn12 cluster, the simplified model depicted in Fig. 3a has been employed. In this model, four $s = 2$ spins, characterized by their effective magnetic anisotropy, and a central fictitious $s = 2$ are ferromagnetically coupled. What is important to note here is that the external spins do not lie on the C_4 axis and, therefore, their easy axis, indicated as an elongated ellipsoid in Fig. 3a, is tilted from the symmetry axis. The angle of tilting, θ , is determined by the orientation of the Jahn–Teller elongation of the Mn(III) coordination site. Abandoning the giant-spin approximation used up to now, the spin Hamiltonian of this model multi-spin system becomes:

$$\mathcal{H} = J \left[\left(\sum_{i=1,4} \mathbf{s}_i \cdot \mathbf{s}_5 \right) + \mathbf{s}_1 \cdot \mathbf{s}_2 + \mathbf{s}_2 \cdot \mathbf{s}_3 + \mathbf{s}_3 \cdot \mathbf{s}_4 + \mathbf{s}_1 \cdot \mathbf{s}_4 \right] + \sum_{i=1,4} \mathbf{s}_i \cdot \mathbf{R}_i \cdot \mathbf{D}_{Mn^{III}} \cdot \mathbf{R}_i^{-1} \cdot \mathbf{s}_i + \mathbf{s}_5 \cdot \mathbf{D}' \cdot \mathbf{s}_5 + \mu_B \sum_{i=1,5} \mathbf{B} \mathbf{g}_i \cdot \mathbf{s}_i \quad (3)$$

where J is the isotropic exchange parameter, \mathbf{R}_i are the matrices representing the symmetry operations of the S_4 point group relating the equivalent Mn sites in the molecules, and $\mathbf{D}_{Mn^{III}}$ are the second-order ZFS tensor of the individual $s = 2$ sites. The numbering scheme is the same as in Fig. 3a.

In Fig. 3b, we show the calculated resonance fields for the four highest-field resonance lines. Interestingly, the second-highest-field transition is calculated to be almost isotropic as experimentally found. The reproduction of this unusual feature of the ESR spectra of Mn12tba suggests that the origin of the transverse anisotropy in this axial molecule can be found in the tilting of anisotropy axes combined with the moderate exchange interaction between the magnetic centers, which break the giant-spin approximation. The transverse anisotropy, and, consequently, the quantum effects in the magnetization dynamics of SMM, are, therefore, dominated by the multi-spin nature of these objects. This observation gives the possibility to rationalize their properties through the exploitation of magneto-structural correlations and opens the perspective to tailor the magnetic anisotropy of SMMs up to higher orders.

3. Spin dynamics in $S = 1/2$ Heisenberg chains with a staggered transverse field

Low-dimensional quantum magnets serve as model systems for investigating numerous fascinating phenomena in materials with cooperative ground states, in particular, induced by high magnetic fields. An $S = 1/2$ Heisenberg antiferromagnetic (AF) chain with exchange interaction J is one of the simplest, but probably the most important model system to study such phenomena. The zero-field ground state of an isotropic $S = 1/2$ Heisenberg AF chain with uniform nearest-neighbor exchange coupling is a spin singlet, and its spin dynamics is determined by a gapless two-particle continuum of fractional $S = 1/2$ excitations, called spinons. Application of an external magnetic field, H , results in a pronounced rearrangement of magnetic excitations, making the spectrum incommensurate but leaving the spinon continuum gapless [12]. The presence of an alternating g -tensor or Dzyaloshinskii–Moriya (DM) interaction can significantly modify the physical properties of spin chains. Such a system can be mapped to a simple Heisenberg chain with a staggered transverse field $h = cH$ [13–15], described by the effective spin Hamiltonian

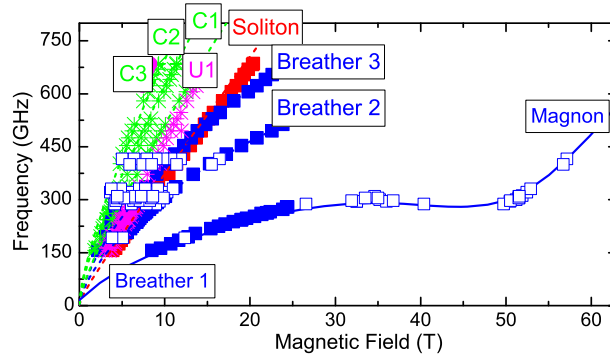


Fig. 4. (Color online) Frequency–field dependence of ESR modes in Cu-PM [22]. Experimental data are denoted by symbols, and the solid line corresponds to results obtained by use of DMRC calculations. Data denoted by closed symbols are taken from Ref. [19], while open symbols are experimental results obtained using the pulsed-field ESR facilities at HLD. Experiments were performed at a temperature of 1.9 K.

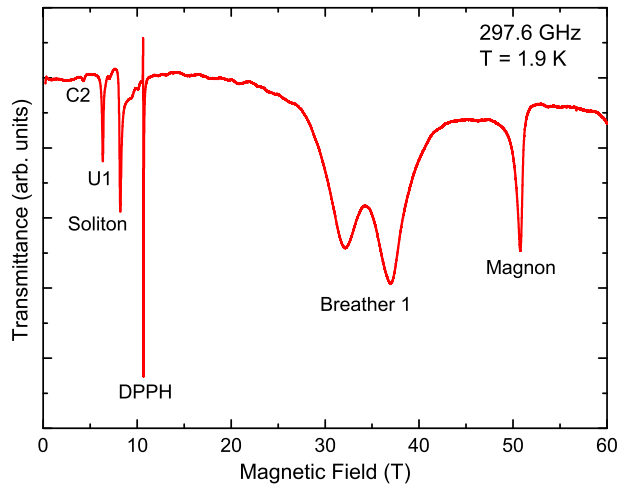


Fig. 5. (Color online) The ESR transmission spectrum of Cu-PM, taken at a frequency of 297.6 GHz at $T = 1.9$ K.

$$\mathcal{H} = \sum_j [J\mathbf{S}_j \cdot \mathbf{S}_{j+1} - HS_j^z - h(-1)^j S_j^x] \quad (4)$$

The sine-Gordon quantum field theory [13–15] applied for this model predicts that the elementary excitation spectrum is to be formed by solitons and their multiple bound states (breathers), with the field-induced energy gap $\Delta \propto H^{2/3}$ determined by the first breather mode. However, in a spin-polarized phase, $H > H_{sat}$, the excitation spectrum is formed by ordinary spin waves (magnons). A pronounced change of the field-induced gap behavior was predicted to take place in the vicinity of H_{sat} [16,17].

The presence of solitons and breathers in the quantum sine-Gordon $S = 1/2$ AF chain material copper pyrimidine dinitrate ([pyrimidine- $\text{Cu}(\text{NO}_3)_2(\text{H}_2\text{O})_2$] $_n$; hereafter Cu-PM) [18] has been confirmed by ESR in magnetic fields up to 25 T [19]. The experiments were done at the National High Magnetic Field Laboratory, Tallahassee, FL, USA, with magnetic field applied along the c'' direction, which is characterized by the maximal value of the staggered magnetization [18]. The corresponding data are compiled in Fig. 4 using filled symbols. In addition to the soliton and three breather modes, several more ESR modes were observed in the magnetic excitation spectra, including the ones labeled by C1–C3 (which correspond to the edges of the soliton–breather continua) and the mode U1, which can be related to bound states due to topological edge effects. The saturation field for Cu-PM, $H_{sat} = 48.5$ T, is known from pulsed-field magnetization measurements [20].

Pulsed-field ESR experiments of Cu-PM were performed at the Dresden High Magnetic Field Laboratory (Hochfeld-Magnetlabor Dresden, HLD at the Helmholtz-Zentrum Dresden-Rossendorf, HZDR) using a pulsed-field ESR spectrometer [21] equipped with VDI diodes (product of Virginia Diodes Inc.) as tunable sources of millimeter-wave radiation and a transmission-type probe in the Faraday configuration. An 8.5 MJ/70 T magnet was employed to generate pulsed magnetic fields with pulse-field rise time of 35 ms and a full-pulse duration of ~ 200 ms. 2,2-Diphenyl-1-Picrylhydrazyl (known as DPPH) was used for calibration of the magnetic field. The resulting data for Cu-PM are shown in Fig. 4 by open symbols [22]. An example of an ESR transmittance spectrum taken at a frequency of 297.6 GHz at $T = 1.9$ K is shown in Fig. 5.

In the absence of a staggered field, the system is gapless below $H = H_{sat}$, and it is in the fully spin-polarized state above. In that state ($H > H_{sat}$), elementary excitations are magnons, and the gap opens linearly with $H - H_{sat}$. Contrary to that, the presence of a staggered field perpendicular to the external field breaks the rotational symmetry around the field and, as consequence, opens a gap in the excitation spectrum. Close to saturation, the spins are almost polarized, and the system cannot develop a large transverse staggered magnetization. So the staggered field is less efficient to open a gap close to saturation than at low field, that determines the different scalings of the gap with c at low field ($\Delta \propto c^{2/3}$) and close to saturation ($\Delta \propto c^{4/5}$). For small enough c , this leads to a minimum of the gap around the saturation field. This explains the small but still well-resolved dip in the frequency–field dependence of magnetic excitations in Cu-PM in the vicinity of H_{sat} .

Results of Density Matrix Renormalization Group (DMRG) calculations for the microscopic model of Eq. (4) with $c = 0.083$ are shown in Fig. 4 by the solid line. The agreement between the DMRG results based on the microscopic model of Eq. (4) and the experimental results is excellent at *all* values of the field including H_{sat} and above [22].

4. New trends in high-field THz resonance spectroscopy

From experimental point of view, a number of ways to study spectroscopic properties of solids in high magnetic fields are possible. The use of different experimental techniques is essentially based on the magnetic fields available: static or transient (pulsed). The employment of far-infrared (FIR) Fourier-transform spectrometers appears very efficient for the broad-band THz spectroscopy in static magnetic fields. Pulsed-field experiments, due to the relatively short field-pulse duration (typically, from 10 to 500 ms), prohibit the use of Fourier-transform spectrometers. Instead, monochromatic radiation sources may be used. During the field pulse, the intensity of the light transmitted through (or reflected from) a sample located in the center of a magnetic field is recorded by fast photo-detectors or hot-electron bolometers. Molecular lasers, either CO (producing radiation with the wavelength of 5 μm) or CO₂ (10 μm), optically pumped FIR Fabry–Perot cavities (70–1200 μm), as well as Backward-Wave Oscillators (BWOs, 30 GHz–1.4 THz) are typically used for THz spectroscopy in pulsed magnetic fields. The development of quantum cascade lasers (QCLs) operating in the THz range has opened the possibility to enlarge the range of excitation energies (4.5–103 μm) and to partly get rid of some critical drawbacks of the optically pumped FIR cavities. Pulsed-field THz spectroscopy has been widely used to investigate the conduction- and valence-band states in bulk semiconductors as well as two-dimensional electron gases (2DEG) in quantum wells (QW) and heterostructures [23–30] through CR experiments. Very recent work has been focused on the investigation of the electronic states in graphite [31,32] and in the ultimate 2DEG in graphene [33–37].

THz-range time-domain (TD) spectroscopy has been employed to study two-dimensional electron gas in steady magnetic fields [38–40]. The possibility of THz TD spectroscopy, based on femtosecond lasers, allows for a broad-band spectroscopy in magnetic fields with long pulse durations (>300 ms). In that case, one of the most challenging tasks is necessary long acquisition time required due to the slow mechanical scanning of the element, which monitors the delay between the pump and the probe femtosecond pulses. A proposed solution employs a fast rotary delay line allowing for high speed THz TD spectroscopy. The feasibility of this approach has been demonstrated by measurements of CR of holes in *p*-doped germanium (Fig. 6) [41].

It is well known that the Ge valence band can be described by two effective masses giving rise to two cyclotron-resonance absorption peaks that shift linearly in frequency with a magnetic field ($\omega_c = eB/m^*$). Two major absorption lines are clearly visible in the lower part of Fig. 6. These lines provide, after scaling, light and heavy hole effective masses of $0.04m_0$ and $0.3m_0$, respectively, in fairly good agreement with previous results. The linear dependence of the resonance frequency versus the applied magnetic field is verified as shown in Fig. 7. Using this experimental approach, pulsed-field time-domain THz spectroscopy is coming close to the capability of static-field measurements and, thus, could be used for wide-band spectroscopy, opening the possibility towards direct measurements of the complex optical conductivity and dielectric constants in very high magnetic fields.

The successful use of the step-scan TD spectroscopy in pulsed magnetic fields has been recently demonstrated by Molter et al. [42]. The setup combines a tabletop 10 T pulsed magnet and a standard THz TD spectroscopy system. The new approach is based on repetitive operation of the pulsed magnet and step-wise increment of the delay time of the TD spectrometer.

Another approach to extend the frequency range of spectrometers used to study resonance phenomena in steady as well as in pulsed magnetic fields is the employment of tunable-frequency THz-range free electron lasers (FEL). Although the idea of using FELs as THz radiation sources in magnetic resonance techniques seems, at the first glance, very straightforward and some attempts have been already made [43–46], until recently it has remained questionable whether a sufficiently high resolution required for most ESR applications (at least better than 1%) can be achieved. It is worth to mention that in contrast to radiation produced by conventional sources (for instance, Gunn-diodes) employed for continuous-wave (cw) ESR spectroscopy, the FELs are operating in a pulsed regime. Due to the Fourier-limited pulse nature, the FEL radiation is not ideally monochromatic – particularly in the case of linac-based FELs. An FEL-based ESR spectrometer which can be operated in pulsed magnetic fields up to 70 T has been recently built at the Dresden High Magnetic Field Laboratory [21]. In this spectrometer, two linac-based FELs are employed as tunable sources of THz radiation for high-field multi-frequency ESR. The spectrometer operates in the quasi-cw mode and allows for ESR experiments in the frequency range of 1.2–75 THz with a spectral resolution better than 1%.

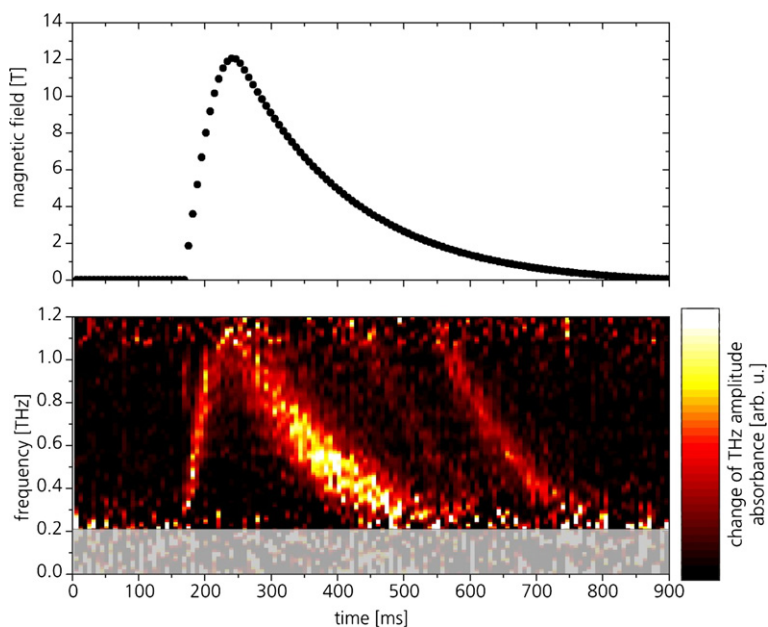


Fig. 6. (Color online) Measured magnetic-field pulse (top) and resulting absorption intensity as a function of time (bottom) [41]. THz radiation absorption versus time, in a wide frequency range from 0.2 to 1.2 THz, was obtained by the Fourier transformation of 150 spectra recorded immediately before and during a single field sweep. The low-frequency part is grayed out due of a poor signal-to-noise ratio.

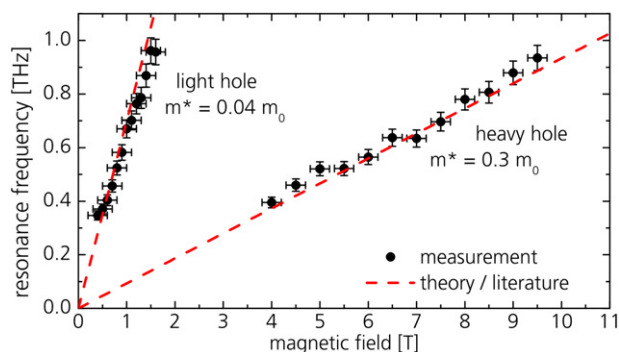


Fig. 7. (Color online) Cyclotron frequency extracted from THz TD spectroscopy data as a function of applied pulsed magnetic field [41].

Both of FELs employed in this setup are Compton FELs working in the upper region of the low-gain regime ($G \sim 10\text{--}80\%$). A mid-infrared (IR) FEL (undulator U27) can be operated in the wavelength range of 4–22 μm , using an electron beam energy varying from 15 to 35 MeV. A long-wavelength far-IR FEL (undulator U100) is equipped with a partially waveguided resonator and can be operated in the wavelength range of 18–250 μm . Thus, the combination of two FELs allows to quasi-continuously cover the wavelength range from 4 to 250 μm . Driven by a superconducting linac, the facility continuously generates radiation pulses with a repetition rate of 13 MHz. The possibility to operate in the quasi-cw regime is one of the most important advantages of FELBE. This regime is of particular importance for pulsed-field ESR (with a typical magnetic field-pulse duration from tens to some hundreds of ms), allowing to avoid complex problems of synchronization of FEL radiation and magnetic-field pulses, permitting longer acquisition times and thus better signal-to-noise ratio. In Table 1, parameters of both FELs are shown.

For the ESR experiments two types of pulsed-field magnets, 8.5 MJ/70 T and 1.4 MJ/60 T, were used [47–49]. The 8.5 MJ/70 T coil has a bore with a diameter of 24 mm, outer diameter 320 mm and can produce magnetic fields up to 70 T. The calculated field homogeneity in the center of the field is better than 7×10^{-4} over 1 cm DSV (diameter spherical volume). This magnet has a pulsed-field rise time of 35 ms, while by using different crowbar resistors the full-pulse duration can be changed approximately from 150 to 300 ms. A maximal peak current is 23.5 kA. The typical waiting time between high-field pulses required for temperature relaxation of this coil is about 3 hours. ESR experiments can be performed also with a smaller, 60 T, coil (1.4 MJ/60 T), with the bore diameter of 24 mm and with a typical full-pulse duration of 40–50 ms. The advantage of using smaller coils is the shorter temperature relaxation time (about 1 hour).

Table 1
FEL specifications.

Parameter	U27	U100
Undulator period (mm)	27.3	100
Number of periods N_u	2×34	38
Undulator parameter K_{rms}	0.3–0.7	0.5–2.7
Wavelength (μm)	4–22	18–250
Pulse durations (ps)	0.9–4	5–30
Max. pulse energy (μJ)	2	5
Max. aver. power (W)	30	65

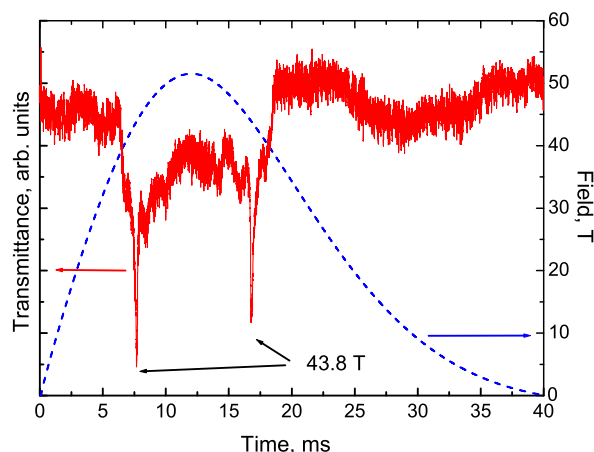


Fig. 8. (Color online) FIR transmittance of $(\text{C}_6\text{H}_9\text{N}_2)\text{CuCl}_3$ (obtained at a frequency of 1.31 THz, at a temperature of 80 K) and magnetic field (shown by the dashed line) vs time [21]. Two sharp absorption lines at 43.8 T corresponding to ESR during the up and down field sweeps are observed. The maximum of the field is 52 T. The 1.4 MJ/60 T magnet was used.

The broad frequency range of the radiation demands several types of detectors. For the long-wavelength range of the FEL radiation (down to 200 μm), a fast hot-electron magnetically-detuned InSb bolometer (product of “QMC Instrument Ltd”) with the time constant of the order of 1 μs was used. For the shorter wavelength range (down to $\sim 30 \mu\text{m}$) a Ge:Ga photoconducting detector (product of “QMC Instrument Ltd”) was employed. This detector has a larger time constant, of the order of milliseconds, but is suitable for ESR experiments in the combination with mid-pulse magnets. For operations in the wavelength range of 4–30 μm a liquid-nitrogen cooled HgCdTe (MCT) photovoltaic detector (model J15D26-M204-S01M-60, product of “Teledyne Judson Technologies”) with a time constant of 80 ns was used.

As mentioned, spectral resolution is one of the most important parameters in ESR spectroscopy, determined by two main factors: (i) monochromaticity of the electromagnetic radiation (in this case defined by the spectral distribution of FEL radiation power due to its Fourier-limited pulsed nature) and (ii) homogeneity of magnetic field. Due to the relatively high-field homogeneity of the used magnet the monochromaticity of the electromagnetic radiation should be regarded as the main parameter determining the spectral resolution of the spectrometer. A spectral resolution better than 1% has been proven by measuring spectra of DPPH (2,2-diphenyl-1-picrylhydrazyl), which is known ESR standard. As examples, the ESR spectrum of the organic quantum spin-1/2 chain compound $(\text{C}_6\text{H}_9\text{N}_2)\text{CuCl}_3$ (also known as 6MAPCuCl₃) obtained at a frequency of 1.31 THz and at a temperature of 80 K is shown in Fig. 8 [21]. Two sharp ESR absorption dips correspond to excitations of exchange-coupled Cu^{2+} centers at 43.8 T during the up and down sweeps of the pulsed field.

Pulsed-field FEL facilities at the HZDR have been also successfully used to study the cyclotron resonance in strained p-InGaAs/GaAs [50] and Ge/Si_{1-x}Ge_x [51], and to probe the photoconductivity of a gallium doped germanium crystals [52]. It is important to mention that the frequency range of the FEL spectrometer (1.2–75 THz) can be extended by use of conventional mm- and submm-wavelength radiation sources (including BWOs, MVNA, Gunn-diodes, etc.) available at the HLD. Employment of these radiation sources allows for multiple frequency ESR experiments in the frequency range from 30 GHz to 1.3 THz, complementing the ESR facility in the low-frequency range (Section 3).

5. Summary

In conclusion, the use of high-field resonance spectroscopy in the THz frequency range has been demonstrated. This technique can be regarded as a very powerful tool to study magnetic excitations in a broad range of materials. The extension of THz spectroscopy techniques in high magnetic field (including the use of pulsed fields) appears to be particularly important, providing unmatched capability to obtain direct information on important physical parameters and magnetic properties of different systems, including those exhibiting high-field-induced phase transitions.

Acknowledgements

A.-L.B. and R.S. particularly acknowledge the long-lasting collaboration with Prof. D. Gatteschi and his contribution to the work reported here. S.A.Z. would like to acknowledge the contribution of E. Čížmár, M. Ozerov, and J. Wosnitza to this work (Sections 3, 4) and the support of the DFG and EuroMagNET II (EU Contract No. 228043).

References

- [1] D. Gatteschi, R. Sessoli, J. Villain, *Molecular Nanomagnets*, Oxford University Press, Oxford, UK, 2006.
- [2] D. Gatteschi, A.L. Barra, A. Caneschi, A. Cornia, R. Sessoli, L. Sorace, *Coord. Chem. Rev.* 250 (2006) 1514.
- [3] S. Hill, R.S. Edwards, N. Aliaga-Alcalde, G. Christou, *Science* 302 (2003) 1015.
- [4] S. Takahashi, I.S. Tupitsyn, J. van Tol, C.C. Beedle, D.N. Hendrickson, P.C.E. Stamp, *Nature* 476 (2011) 76.
- [5] W. Wernsdorfer, M. Murugesu, G. Christou, *Phys. Rev. Lett.* 96 (2006) 057208.
- [6] S. Hill, N. Anderson, A. Wilson, S. Takahashi, K. Petukhov, N.E. Chakov, M. Murugesu, J.M. North, E. Del Barco, A.D. Kent, N.S. Dalal, G. Christou, *Polyhedron* 24 (2005) 2284.
- [7] A.L. Barra, D. Gatteschi, R. Sessoli, *Phys. Rev. Lett.* 56 (1997) 8192.
- [8] A.L. Barra, A. Caneschi, A. Cornia, D. Gatteschi, L. Gorini, L.P. Heiniger, R. Sessoli, L. Sorace, *J. Am. Chem. Soc.* 129 (2007) 10754.
- [9] R.J. Elliott, K.W.H. Stevens, *Proc. Royal Soc. A, Math. Phys. Sci.* 218 (1953) 553.
- [10] A.L. Barra, D. Gatteschi, R. Sessoli, *Chem. Eur. J.* 6 (2000) 1608.
- [11] R. Caciuffo, G. Amoretti, A. Murani, R. Sessoli, A. Caneschi, D. Gatteschi, *Phys. Rev. Lett.* 81 (1998) 4744.
- [12] G. Müller, H. Thomas, H. Beck, J.C. Bonner, *Phys. Rev. B* 24 (1981) 1429.
- [13] F.H.L. Essler, *Phys. Rev. B* 59 (1999) 14376.
- [14] M. Oshikawa, I. Affleck, *Phys. Rev. Lett.* 79 (1997) 2883.
- [15] I. Affleck, M. Oshikawa, *Phys. Rev. B* 60 (1999) 1038; I. Affleck, M. Oshikawa, *Phys. Rev. B* 62 (2000) 9200.
- [16] J.Z. Zhao, X.Q. Wang, T. Xiang, Z.B. Su, L. Yu, *Phys. Rev. Lett.* 90 (2003) 207204.
- [17] J.-B. Fouet, O. Tchernyshyov, F. Mila, *Phys. Rev. B* 70 (2004) 174427.
- [18] R. Feyerherm, S. Abens, D. Günther, T. Ishida, M. Meißner, M. Meschke, T. Nogami, M. Steiner, *J. Phys.: Condens. Matter* 12 (2000) 8495.
- [19] S.A. Zvyagin, A.K. Kolezhuk, J. Krzystek, R. Feyerherm, *Phys. Rev. Lett.* 93 (2004) 027201.
- [20] A.U.B. Wolter, H. Rakoto, M. Costes, A. Honecker, W. Brenig, A. Klümper, H.-H. Klauss, F.J. Litterst, R. Feyerherm, D. Jérôme, S. Süllow, *Phys. Rev. B* 68 (2003) 220406(R).
- [21] S.A. Zvyagin, M. Ozerov, E. Čížmár, D. Kamenskyi, S. Zherlitsyn, T. Herrmannsdörfer, J. Wosnitza, R. Wünsch, W. Seidel, *Rev. Sci. Instrum.* 80 (2009) 073102.
- [22] S.A. Zvyagin, E. Čížmár, M. Ozerov, J. Wosnitza, R. Feyerherm, S.R. Manmana, F. Mila, *Phys. Rev. B* 83 (2011) 060409(R).
- [23] A.V. Ikonnikov, K.E. Spirin, V.I. Gavrilenko, D.V. Kozlov, O. Drachenko, H. Schneider, M. Helm, *Semiconductors* 44 (2010) 1492.
- [24] O. Drachenko, A. Patane, N.V. Kozlova, Q.D. Zhuang, A. Krier, L. Eaves, M. Helm, *Appl. Phys. Lett.* 98 (2011) 162109.
- [25] A.V. Ikonnikov, M.S. Zholudev, K.E. Spirin, A.A. Lastovkin, K.V. Maremyanin, V.Ya. Aleshkin, V.I. Gavrilenko, O. Drachenko, M. Helm, J. Wosnitza, M. Goiran, N.N. Mikhailov, S.A. Dvoretiskii, F. Tepe, N. Diakonova, C. Consejo, B. Chenaud, W. Knap, *Semicond. Sci. Technol.* 26 (2011) 125011.
- [26] O. Drachenko, S. Winnerl, H. Schneider, M. Helm, J. Wosnitza, J. Léotin, *Rev. Sci. Instrum.* 82 (2011) 033108.
- [27] A. Patané, W.H.M. Feu, O. Makarovskiy, O. Drachenko, L. Eaves, A. Krier, Q.D. Zhuang, M. Helm, M. Goiran, G. Hill, *Phys. Rev. B* 80 (2009) 115207.
- [28] W. Knap, S. Contreras, H. Alause, J. Camassel, M. Dyakonov, J.L. Robert, J. Yang, Q. Chen, M. Asif Khan, M.L. Sadowski, S. Huant, F.H. Yang, M. Goiran, J. Léotin, M.S. Shur, *Appl. Phys. Lett.* 70 (1997) 16.
- [29] M.P. Semtsiv, O. Bierwagen, W.T. Masselink, M. Goiran, J. Galibert, J. Léotin, *Phys. Rev. B* 77 (2008) 16.
- [30] O. Drachenko, D.V. Kozlov, V.Ya. Aleshkin, V.O. Gavrilenko, K.V. Maremyanin, A.V. Ikonnikov, B.N. Zvonkov, M. Goiran, J. Léotin, G. Fasching, S. Winnerl, H. Schneider, J. Wosnitza, M. Helm, *Phys. Rev. B* 79 (2009) 073301.
- [31] K.-C. Chuang, A.M.R. Baker, R.J. Nicholas, *Phys. Rev.* 80 (2009) 161410(R).
- [32] M. Orlita, P. Neugebauer, C. Faugeras, A.-L. Barra, M. Potemski, F.M.D. Pellegrino, D.M. Basko, *Phys. Rev. Lett.* 108 (2012) 017602.
- [33] Z. Jiang, E.A. Henriksen, L.C. Tung, Y.-J. Wang, M.E. Schwartz, M.Y. Han, P. Kim, H.L. Stormer, *Phys. Rev. Lett.* 98 (2007) 197403.
- [34] M. Orlita, C. Faugeras, G. Martinez, D.K. Maude, M.L. Sadowski, M. Potemski, *Phys. Rev. Lett.* 100 (2008) 136403.
- [35] M. Orlita, C. Faugeras, J.M. Schneider, G. Martinez, D.K. Maude, M. Potemski, *Phys. Rev. Lett.* 102 (2009) 166401.
- [36] E.A. Henriksen, P. Cadden-Zimansky, Z. Jiang, Z.Q. Li, L.C. Tung, M.E. Schwartz, M. Takita, Y.-J. Wang, P. Kim, H.L. Stormer, *Phys. Rev. Lett.* 104 (2010) 067404.
- [37] L.G. Booshehri, C.H. Mielke, D.G. Rickel, S.A. Crooker, Q. Zhang, L. Ren, E.H. Házro, A. Rustagi, C.J. Stanton, Z. Jin, Z. Sun, Z. Yan, J.M. Tour, J. Kono, *Phys. Rev. B* 85 (2012) 205407.
- [38] X. Wang, D. Hilton, D.J.L. Reno, D.M. Mittleman, J. Kono, *Opt. Lett.* 32 (2007) 1845.
- [39] X. Wang, D. Hilton, D.J.L. Reno, D.M. Mittleman, J. Kono, *Opt. Express* 18 (2010) 12354.
- [40] T. Arikawa, X. Wang, D.J. Hilton, J.L. Reno, W. Pan, J. Kono, *Phys. Rev. B* 84 (2011) 241307(R).
- [41] D. Molter, F. Ellrich, T. Weinland, S. George, M. Goiran, F. Keilmann, R. Beigang, J. Léotin, *Opt. Express* 18 (2010) 26163.
- [42] D. Molter, G. Torosyan, G. Ballon, L. Drigo, R. Beigang, J. Léotin, *Opt. Express* 20 (2012) 5993.
- [43] T.A. Vaughan, R.J. Nicholas, C.J.G.M. Langerak, B.N. Murdin, C.R. Pidgeon, N.J. Mason, P.J. Walker, *Phys. Rev. B* 53 (1996) 16481.
- [44] L. Van Bockstal, L. Li, C.J.G.M. Langerak, M.J. van de Pol, A. De Keyser, A.F.G. van der Meer, A. Ardavan, J. Singleton, R.J. Nicholas, F. Herlach, R. Bogaerts, H.U. Mueller, M. von Ortenberg, *Physica B* 246–247 (1998) 208.
- [45] C.J.G.M. Langerak, L. Li, L. Van Bockstal, A. Ardavan, M.J. van de Pol, A.F.G. van der Meer, F. Herlach, H.U. Mueller, R.J. Nicholas, J. Singleton, *Physica B* 246–247 (1998) 400.
- [46] C.J.G.M. Langerak, J. Singleton, L. Li, L. Van Bockstal, A. Ardavan, M.J. van de Pol, A.F.G. van der Meer, F. Herlach, N. Mason, R.J. Nicholas, P.J. Walker, *Physica B* 256 (1998) 339.
- [47] S. Zherlitsyn, T. Herrmannsdörfer, Yu. Skourski, A. Sytcheva, J. Wosnitza, *J. Low Temp. Phys.* 146 (2007) 719.
- [48] S. Zherlitsyn, A.D. Bianchi, T. Herrmannsdörfer, F. Pobell, Yu. Skourski, A. Sytcheva, S. Zvyagin, J. Wosnitza, *IEEE Trans. Appl. Supercond.* 16 (2006) 1660.
- [49] J. Wosnitza, G. Goll, M. Bartkowiak, B. Bergk, A.D. Bianchi, H.v. Lohneysen, T. Yoshino, T. Takabatake, *Physica B: Condens. Matter* 403 (2008) 1219.
- [50] O. Drachenko, D.V. Kozlov, V.Ya. Aleshkin, V.I. Gavrilenko, K.V. Maremyanin, A.V. Ikonnikov, B.N. Zvonkov, M. Goiran, J. Léotin, G. Fasching, S. Winnerl, H. Schneider, J. Wosnitza, M. Helm, *Phys. Rev. B* 79 (2009) 073301.
- [51] N. Miura, N. Kozlova, K. Dorr, J. Freudenberger, L. Schultz, O. Drachenko, K. Sawano, Y. Shiraki, *J. Low Temp. Phys.* 159 (2010) 222.
- [52] O. Drachenko, H. Schneider, M. Helm, D. Kozlov, V. Gavrilenko, J. Wosnitza, J. Léotin, *Phys. Rev. B* 84 (2011) 245207.